actuators

MDPI

Article

Wireless Hybrid-Actuated Soft Miniature Robot for Biomedical Applications

Heera Kim †, Kyongsu Lee † and Gwangjun Go *

Department of Mechanical Engineering, Chosun University, 309 Pilmun-daero, Dong-gu, Gwangju 61452, Republic of Korea; khr2747@chosun.kr (H.K.); lgs3326@chosun.kr (K.L.)
* Correspondence: gwangjungo@chosun.ac.kr
† These authors contributed equally to this work.

Abstract: Wireless soft miniature robots have been studied for biomedical applications. However, the wireless soft miniature robots developed so far are mainly composed of synthetic polymers that do not guarantee biocompatibility and biodegradability. Additionally, current soft robots have limitations in demonstrating mobility in narrow spaces, such as blood vessels within the body, by using their flexible body. This study proposes a wireless hybrid-actuated soft miniature robot for biomedical applications. The proposed soft miniature robot consists of biodegradable chitosan and magnetic nanoparticles (MNPs) and is fabricated into an eight-arm shape by laser micromachining. The soft miniature robot can implement hydrogel swelling and magnetic-actuated shape morphing by using the difference in MNP density and magnetic field responsiveness within the robot body, respectively. Furthermore, the soft miniature robot can be guided by external magnetic fields. As feasibility tests, the soft miniature robot demonstrated on-demand pick-and-place motion, grasping a bead, moving it to a desired location, and releasing it. Furthermore, in an in-channel mobility test, the flexible body of the soft miniature robot passed through a tube smaller in size than the robot itself through magnetically actuated shape morphing. These results indicate that the soft miniature robot with controllable shape change and precise magnetic-driven mobility can be a minimally invasive surgical robot for disease diagnosis and treatment.

Keywords: soft robot; wireless actuation; biomedical application

check for updates

Citation: Kim, H.; Lee, K.; Go, G. Wireless Hybrid-Actuated Soft Miniature Robot for Biomedical Applications. *Actuators* **2024**, *13*, 341. https://doi.org/10.3390/act13090341

Academic Editor: Alessio Merola

Received: 11 August 2024
Revised: 23 August 2024
Accepted: 3 September 2024
Published: 5 September 2024

Copyright: © 2024 by the authors. Licensee MDPI, Basel, Switzerland. This article is an open access article distributed under the terms and conditions of the Creative Commons Attribution (CC BY) license (https://creativecommons.org/licenses/by/4.0/).

1. Introduction

Recently, soft robots have attracted significant attention in various applications, such as medical/healthcare, military, environment, and exploration [1–4]. The soft robots can adapt to irregularly shaped surfaces and harsh environments due to their flexible body structure. Furthermore, soft robots have characteristics that are robust to external impacts and, at the same time, have a significantly low possibility of causing damage to the object being manipulated. Despite the many advantages of soft robots, their use in biomedical applications has been focused on wearable devices outside the body, and their use inside the body still needs to be improved [5].

In order to utilize soft robots in biomedical applications, the soft robot should be non-toxic when inserted into the body and then be excreted or degraded by itself after performing its task [4,6]. In addition, narrow spaces in the body, such as blood vessels, articular cavities, and bile ducts, require flexible locomotion by the robot with a high degree of freedom. Along with the degree of freedom of the robot, the robot's size needs to be kept below the millimeter to move freely in the body space and body fluids. Furthermore, a soft robot wirelessly driven by external, beyond-wire-driven, energy is required.

The development of wirelessly actuated soft miniature robots for disease treatment is actively underway to address the limitations of soft robots (Figure S1) [7–17]. Some of the materials used in the soft robots can respond to various external stimuli, such as magnetic

fields, ultrasound, temperature, humidity, and chemicals (Figure S2). Here, magnetic fields and ultrasound can induce shape morphing of soft miniature robots because they can penetrate the human body without damage, and the response of the soft miniature robot is immediate. However, magnetic fields and ultrasound experience a loss in intensity depending on the distance or the medium in the body, so the shape morphing of the soft miniature robot weakens. Chemicals, temperature, and humidity can induce rapid responses and significant shape changes in soft miniature robots. However, chemicals, temperature, and humidity can directly affect the body, which limits their use in biomedical applications. Therefore, soft miniature robots maximize their advantages in biomedical applications by utilizing magnetic fields and ultrasound alone or by using two or more external stimuli.

To examine the feasibility of soft miniature robots in biomedical applications, the actuation performance of the soft miniature robots has been demonstrated under various external stimuli. For example, Hu et al. developed a soft miniature robot using a magnetic alignment of magnetic particles and elastic composites, which exhibited controllable mobility and flexible shape morphing in response to external magnetic fields [15]. In addition, the soft miniature robot showed various functions applicable to biomedical applications, such as moving in narrow spaces or targeting micro-objects to desired locations. However, materials for biocompatibility and biodegradability have not been applied or verified for soft robots. Therefore, securing the in vivo safety of soft robots remains challenging.

Recognizing these limitations, more recently, soft miniature robots have been studied to consist of biomaterials to ensure biocompatibility and to be excreted or slowly degraded in the body (Figure S1) [18–21]. Soft miniature robots made from biomaterials can move and change shape in response to external energy, similar to non-biomaterials. However, biomaterial-based soft miniature robots developed to date have relatively small maximum bending curvatures, resulting in a lower shape-morphing performance than elastomer-based soft miniature robots. This weak shape morphing hinders the locomotion and flexibility of soft robots, thereby impeding their accessibility to complex and narrow spaces in the body and precisely targeted drug delivery. To enhance the shape morphing of biomaterial-based soft miniature robots, we recently developed a soft miniature robot composed of natural polymer and magnetic nanoparticles [21]. The soft miniature robot exhibited programmable shape deformation and responded rapidly to six stimuli: humidity, chemical solvents, near-infrared (NIR) light, radio frequency (RF) heating, temperature, and magnetic fields. The soft miniature robot had high bending curvature compared to previous studies. In addition, the soft miniature robot demonstrated controllability in moving in a desired direction and location. Despite the magnetic mobility and high shape-morphing performance, the soft robot was limited to showing mobility in wide spaces such as channels and rat abdominal cavities. Therefore, mobility in narrow spaces by utilizing the flexibility of soft robots required for precise targeting of the body has yet to be reported. In addition, the mobility and shape morphing of soft robots by wireless magnetic actuation still need to be clearly analyzed.

This study proposes a wirelessly hybrid-actuated soft miniature robot for biomedical applications. The proposed soft robot consists of chitosan, a natural polymer with biocompatibility, biodegradability, and hydrogel expandability, and magnetic nanoparticles (MNPs) with magnetic response. The wireless actuation of the soft robot is realized by the hydrogel swelling of chitosan and the magnetic response of MNPs (Figure 1a). First, the densely packed MNPs on the bottom of the soft robot cause non-uniform hydrogel expansion of chitosan. Thus, the passive and active layers formed on the soft robot can generate strong bending by water absorption. In addition, the flexible body formed by the water absorption of chitosan helps the soft robot to access narrow spaces in the body. Next, the soft robot's magnetic actuation provides precise targeting and transient morphology changes caused by magnetic force in response to external magnetic fields. Specifically, the magnetic force provides the soft robot's gripping function and thus helps it load the drug-loaded beads (Figure 1b). As shown in Figure 1c, the soft miniature robot traps a

drug-loaded bead through shape morphing actuated by magnetic fields in vitro. Subsequently, the robot is inserted into the body and guided to the target site using magnetic field control. Upon reaching the target site, the drug-loaded bead is released as the soft miniature robot unfolds due to shape morphing. The flexible body, on-demand shape change, and precise targeting of the proposed soft miniature robot can expand the utility of soft robots in biomedical applications.

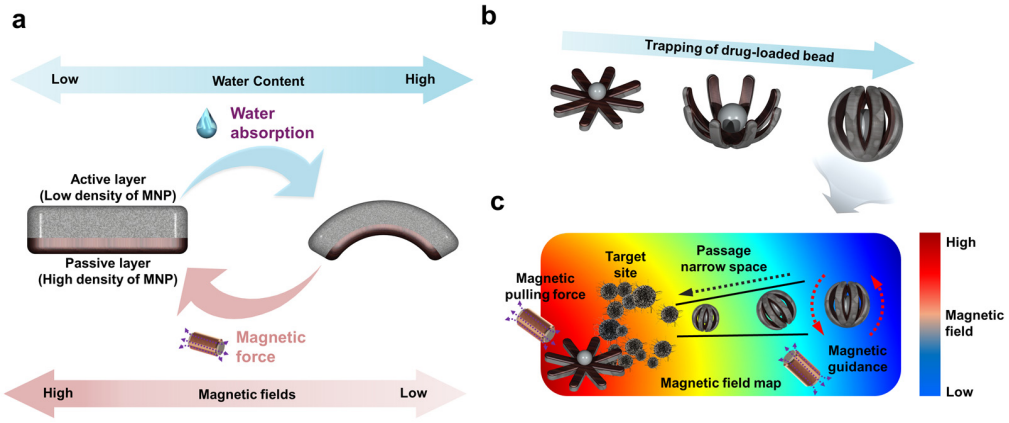

Figure 1. Concept overview of the wireless hybrid-actuated soft miniature robot for biomedical application. (**a**,**b**) Illustration of hydrogel-swelling- and magnetic-fields-based actuation of soft miniature robot. (**c**) Magnetic-field-driven targeted delivery process of the soft miniature robot with drug-loaded bead.

2. Materials and Methods

2.1. Materials

For the fabrication of a soft miniature robot, chitosan (low molecular weight) and Iron (II, III) oxide (Fe_3O_4) nanoparticles (50–100 nm particle size) were obtained from Sigma-Aldrich (St. Louis, MO, USA). Acetic acid was purchased from DUKSAN (Ansan, Republic of Korea). To prepare the alginate bead, sodium alginate and calcium chloride were purchased from Sigma-Aldrich.

2.2. Fabrication of the Soft Miniature Robot

The soft miniature robot was fabricated by preparation of a chitosan sheet containing MNPs (chitosan–MNPs sheet) and laser micromachining of the sheet (Figure S3). The fabrication method was modified from our previous study [18]. First, the chitosan–MNPs sheet was prepared by dissolving chitosan in 2% v/v acetic acid to prepare a 1.5% v/w chitosan solution. Then, 7% v/w MNPs were stirred into the chitosan solution at a warm temperature. The chitosan solution containing 5 mL of MNPs was poured into a 60 mm diameter Petri dish and then dried at 40 °C for more than 3 h. The dried chitosan–MNPs sheet was separated from the Petri dish and stored in a vacuum to prevent contact with air. To obtain a soft miniature robot, the prepared chitosan–MNPs sheet was cut based on three-dimensional (3D) computer-aided design (CAD) drawings by femtosecond pulse laser micromachining using a pulse duration of 90 fs, a wavelength of 343 nm, and a power of 240 mW. In the laser micromachining step of the chitosan–MNPs sheets, a wavelength of 343 nm was applied, considering the high energy absorption wavelength range (300−400 nm) of chitosan [22]. A power of 240 mW was determined to be the optimal value to minimize damage caused by the high energy absorption of chitosan [23]. After laser micromachining, soft miniature robots were separated from the remaining chitosan–MNPs sheets. The obtained soft miniature robots were sequentially immersed in 100% and 70% ethanol solutions and deionized water to remove residual acetic acid. The prepared soft miniature robots were stored in deionized water until used in an actuation test.

2.3. Characterization of the Soft Miniature Robot

The shape of a soft miniature robot was observed using scanning electron microscopy (SEM) (SU8010; HITACHI, Tokyo, Japan) and a digital single-lens reflex (DSLR) camera (EOS 600D, CANON, Tokyo, Japan). For SEM surface analysis, the prepared chitosan–MNPs sheets and soft miniature robots were pretreated through Pt coating and then scanned at a magnification of 100× or more. Next, energy-dispersive X-ray spectrometry (EDX) was used to analyze the density difference in MNPs inside the soft miniature robot. While using the EDX, elemental signal-mapping images were acquired by capturing and constructing the Fe signals emitted from the soft miniature robot. The chemical structures of the chitosan, MNPs, and soft miniature robot were measured using a Fourier transform infrared (FTIR) spectrophotometer (Thermo Nicolet Corporation, Waltham, MA, USA) under 16 scans per sample ranging from 400 cm^{-1} to 4000 cm^{-1} with a resolution of 4 cm^{-1}. The magnetization curves of the chitosan, MNPs, and soft miniature robot were recorded using a vibration sample magnetometer (VSM, Lake Shore Cryotronics 7404, Westerville, OH, USA). To each sample, a magnetic field strength ranging from −1 T to 1 T, generated from the coils of the VSM, was applied at intervals of 40 mT. The magnetic response of the soft miniature robot was evaluated using external magnetic fields generated from an N35 grade neodymium permanent magnet (width 35 mm, length 35 mm, and height 10 mm). The behavior of soft miniature robots as they approached a permanent magnet was captured using a DSLR camera.

2.4. Hydrogel-Swelling- and Magnetic-Fields-Based Shape-Morphing Test of the Soft Miniature Robot

The hydrogel-swelling-actuated bending test of the soft miniature robot was performed in diluted ethanol solutions. Next, the magnetic-field-actuated unfolding test was evaluated using external magnetic fields generated from a single N35-grade neodymium permanent magnet (diameter 10 mm and height 6 mm). Here, the intensity of the external magnetic fields was measured using a Gauss meter (GM-2 Gauss meter, AlphaLab Inc., Salt Lake City, UT, USA), depending on the distance between the magnets. The shape morphing of the soft miniature robot was recorded using a DSLR camera.

2.5. Magnetic-Field-Driven Mobility of the Soft Miniature Robot

The soft miniature robot is guided toward the desired direction by external magnetic fields generated from an electromagnetic navigation system (ENS) and a permanent magnet. Here, the ENS consists of six rectangular electromagnetic coils orthogonally arranged along the x-, y-, and z-axes. The ENS is controlled through LabVIEW 2018 (National Instruments, Austin, TX, USA), and the current of each electromagnetic coil is applied via motor driver controllers (ESCON 70/10, Maxon Motor, Sachseln, Switzerland).

The soft miniature robot generates magnetic torque ($\boldsymbol{\tau}$) and magnetic force ($\mathbf{F}_m$) under the external magnetic fields and gradient as follows:

$$\boldsymbol{\tau} = V\mathbf{M} \times \mathbf{B} \tag{1}$$

$$\mathbf{F}_m = V(\mathbf{M}\cdot\nabla)\mathbf{B} \tag{2}$$

The volume, magnetization, flux density, and gradient of the soft miniature robot are represented by V, $\mathbf{M} \in \mathbf{R}^{3\times1}$, $\mathbf{B} \in \mathbf{R}^{3\times1}$, and ∇, respectively.

In the magnetic-fields-driven mobility of soft miniature robots using the ENS, the rolling motion of the soft miniature robot is realized by rotating a uniform magnetic field generated by six orthogonally arranged rectangular electromagnetic coils, which generates a rotating magnetic field that can be described as follows:

$$\mathbf{B} = \begin{bmatrix} B_x(t) \\ B_y(t) \\ B_z(t) \end{bmatrix} = \begin{bmatrix} B_{0,r}cos\theta coswt \\ B_{0,r}sin\theta coswt \\ B_{0,r}sinwt \end{bmatrix} \tag{3}$$

where the magnetic flux generated by the electromagnetic coils and the rotational angular velocity of the soft miniature robot are represented as $B_{0,r}$ and w, respectively.

To perform bead gripping and release tests, alginate beads were prepared through droplet crosslinking. Specifically, a 3% sodium alginate solution containing blue dye was formed into droplets through a 30-gauge syringe. The droplets were solidified into alginate beads by crosslinking and immersing them in a 10% calcium chloride solution.

3. Results and Discussion

3.1. Characterization of Magnetically Actuated Soft Miniature Robot

A magnetically actuated soft miniature robot was obtained by laser micromachining a chitosan–MNPs sheet (Figure 2a). The prepared chitosan–MNPs sheet has a rough and even morphology on the top and bottom surfaces, respectively, due to the difference in the density of MNPs (Figure 2b,c). In addition, EDX mapping images clearly show the density difference in MNPs (Fe wt%; Top: 10.9% and Bottom: 50.6%) on the top and bottom surfaces of the chitosan–MNPs sheets (Figure 2c). These results reveal that active and passive layers formed, which can be actuated by hydrogel swelling. The soft miniature robot was designed using CAD to have eight arms with a width of 0.3 mm and 25 robots in a 5 × 5 matrix. The eight-arm structure can stably grip the drug-loaded beads when the soft robot is deformed due to hydrogel expansion or magnetic actuation. Based on the designed 2D CAD drawing, the chitosan–MNPs sheet was laser micromachined. As a result, 25 soft miniature robots were obtained, similar to the CAD drawing (Figure 2d), and had eight arms with a width of about 0.26 mm (Figure 2e). Here, the laser micromachining caused an accuracy error of about 20 μm in the robot fabrication. The soft miniature robots had a thickness of about 306.82 ± 33.05 μm (Figure 2f). These results indicate that laser micromachining can be applied as a fabrication method to obtain soft miniature robots by minimizing the damage to the chitosan–MNPs sheet.

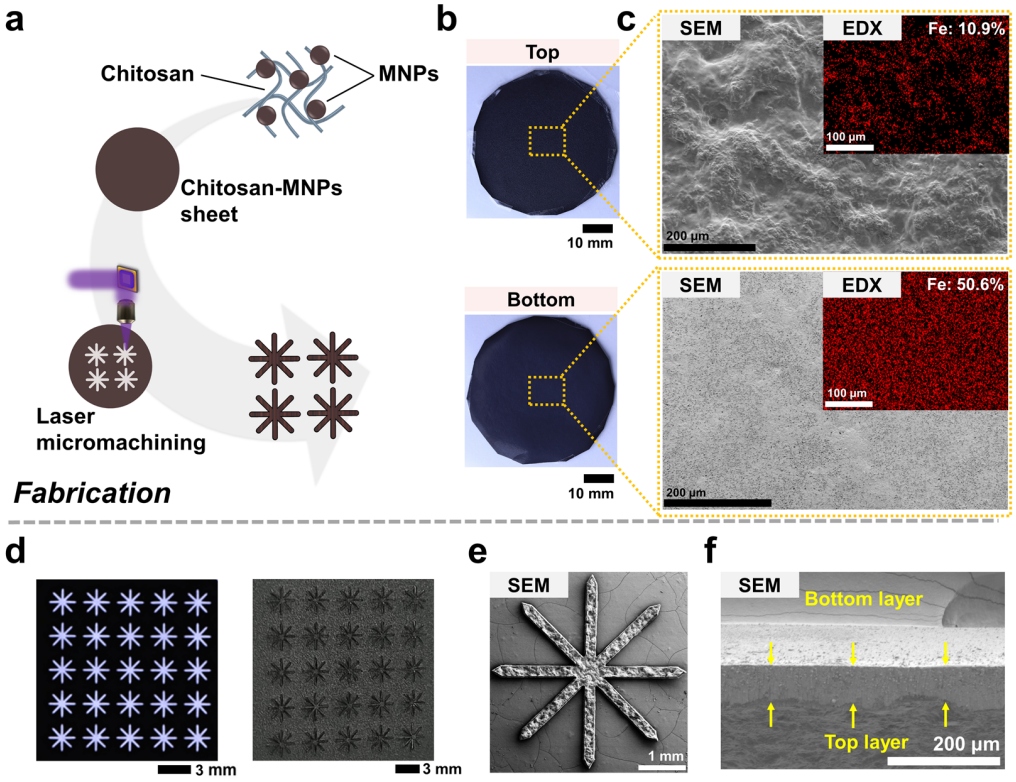

Figure 2. Fabrication and morphological characterization of the soft miniature robot. (**a**) Schematic illustration of the preparation of the soft miniature robot. (**b**) Optical and (**c**) SEM and EDX mapping

images of the top and bottom of the chitosan–MNPs sheet. The red color in the EDX mapping image represents the distribution of the Fe signal detected from the soft miniature robot. (**d**) Optical images showing 25 eight-arm-shaped soft robots fabricated in a 5 × 5 matrix. (**e**,**f**) SEM images showing (**e**) the top and (**f**) cross-section of the soft miniature robot. Arrows indicate the boundaries of the top and bottom of the soft robot.

To investigate the chemical composition of the soft miniature robot, FTIR spectra were tested for the soft miniature robot and its components (Figure 3a). The spectral peaks of the soft miniature robot are consistent with the significant components of chitosan (stretching vibration of the peptide carbonyl group (–C. O) at 1647 cm^{-1} and C–O stretching at 1082 and 1028 cm^{-1}) [24] and MNPs (peak at 570 cm^{-1}) [25]. These FTIR spectra results reveal that the soft miniature robot contains the components without structural modification by chemical bonding.

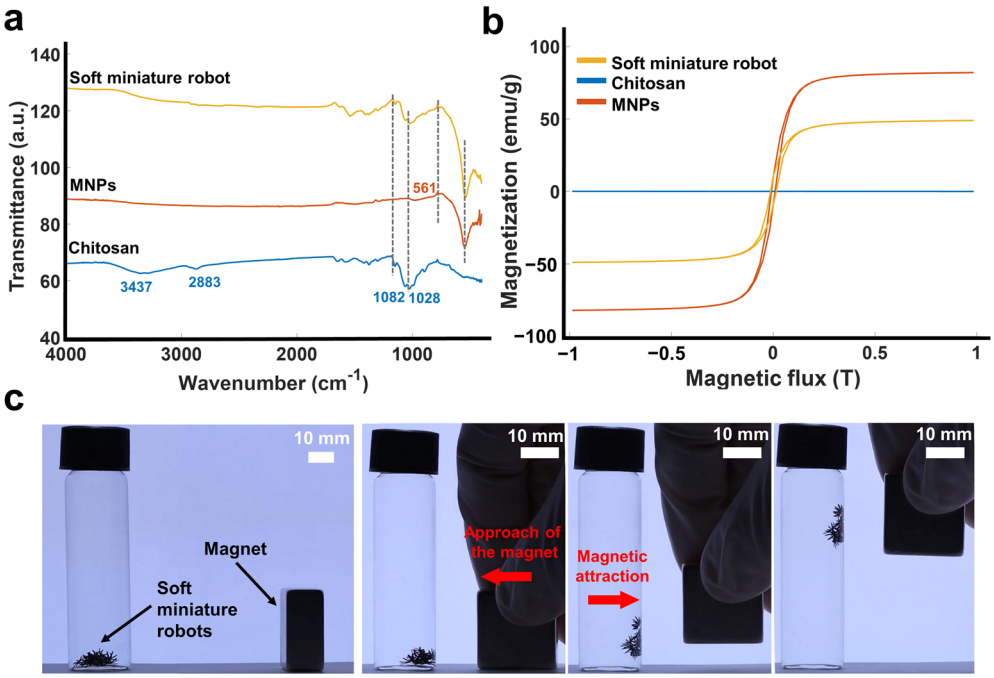

Figure 3. Chemical composition and magnetic response of the soft miniature robot. (**a**) FTIR spectra of chitosan, MNPs, and soft miniature robot. (**b**) Magnetization curve of chitosan, MNPs, and soft miniature robot. (**c**) Magnetic response of soft miniature robots using a permanent magnet.

To test the magnetic response of the soft miniature robot under external magnetic fields, the magnetization curve of the soft miniature robot by external magnetic fields was measured using a VSM (Figure 3b). Among the constituent materials of the soft miniature robot, chitosan has little response to external magnetic fields, but the MNPs have a high magnetized saturation (82 emu/g). Therefore, the magnetization curve of the soft miniature robot shows a lower magnetized saturation (48.9 emu/g) than that of the MNPs due to the influence of chitosan, which has no magnetic response. Next, regarding magnetic field responsiveness, the soft miniature robots are magnetized under an external magnetic field generated from a neodymium permanent magnet. Then, the magnetized soft robots are attracted to the magnet where the magnetic force is generated (Figure 3c). As a result, we confirmed that the soft miniature robots have sufficient magnetic field responsiveness to be actuated by an external magnetic field.

3.2. Hydrogel-Swelling-Actuated Bending of Soft Miniature Robot

The soft miniature robot is designed to enable shape morphing by hydrogel swelling. The shape-morphing mechanism of the soft robot is caused by different instances of hy-

drogel swelling between the top and bottom layers due to the difference in the density of MNPs within the two layers. Using the shape-morphing mechanism, we can manipulate the bending curvature of the soft miniature robot by controlling the water absorption (Figure 4a).

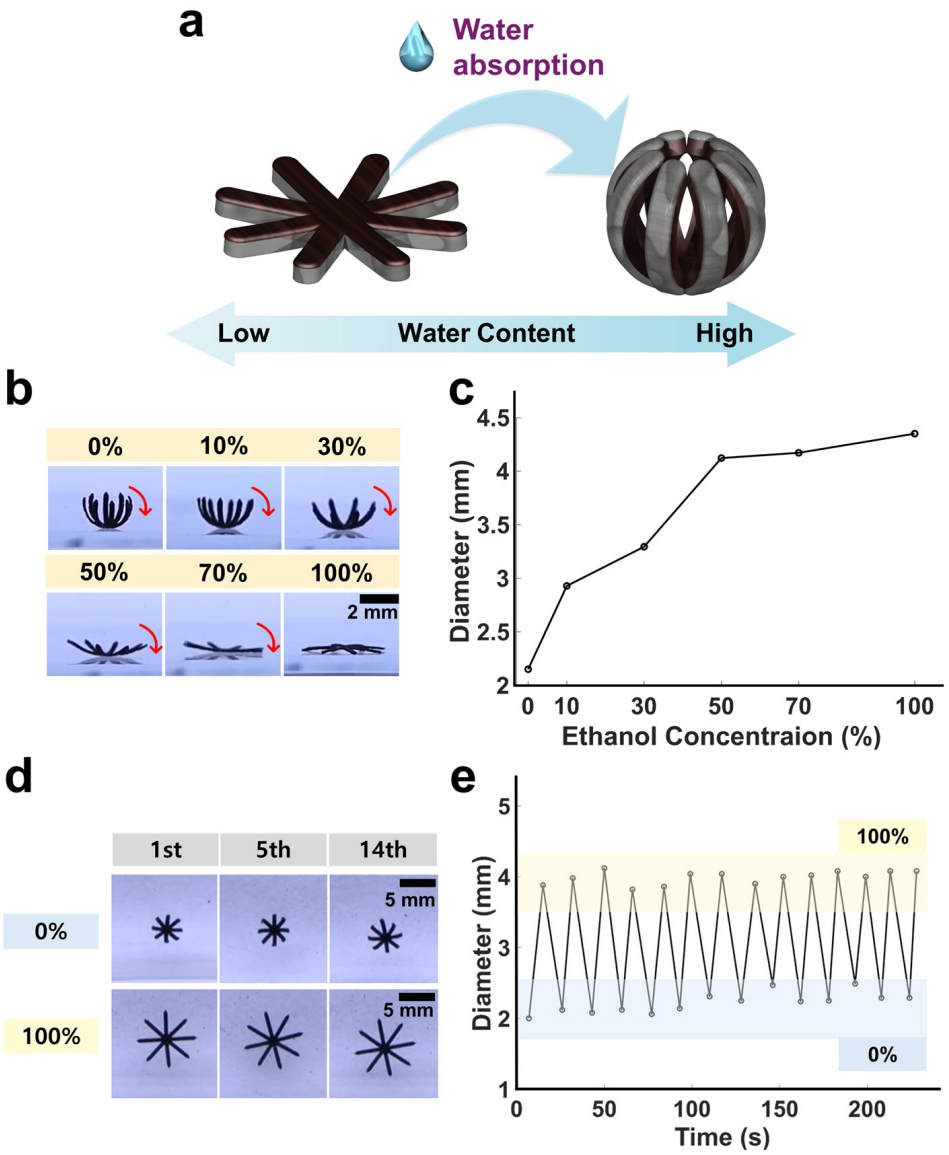

Figure 4. Hydrogel-swelling-actuated bending performance of the soft miniature robot. (**a**) Schematic illustration of hydrogel-swelling-actuated shape morphing of the soft miniature robot. (**b**) Optical images and (**c**) graph showing shape morphing of the soft miniature robot according to water absorption (0%, 10%, 30%, 50%, 70%, and 100% ethanol solutions). In the optical images, the red arrow indicates the deformation direction of the soft miniature robot. (**d**) Optical images and (**e**) graph of the change in the diameter of the soft miniature robot in deionized water (0% ethanol) and 100% ethanol. The yellow and blue boxes depict the diameter of the soft miniature robot in 100% ethanol and deionized water (0% ethanol), respectively.

The shape-morphing control of the soft robot by hydrogel swelling was evaluated according to the water absorption. We treated the soft miniature robot with diluted ethanol solutions (0–100%) to control the water absorption and then observed the bending curvature of the soft robot (Figure 4b). The soft miniature robot was dehydrated in 100% ethanol and then unfolded. After that, as the ethanol solution was gradually diluted with water, the water absorption of the soft miniature robot increased, resulting in a gradually higher

bending curvature. As shown in Figure 4c, the soft miniature robot immersed in deionized water without ethanol has a smaller size (about a diameter of 2.22 mm) than the dehydrated (about a diameter of 4.35 mm) in ethanol. In addition, the maximum bending curvature and angle of the soft miniature robot were ~2 mm and 140° in deionized water (0% ethanol), respectively. Consequently, we inferred that the strong bending of the soft miniature robot by hydrogel-swelling actuation is sufficient to trap drug-loaded microbeads stably.

Next, to evaluate the durability of the soft miniature robot, we observed the shape changes in the soft miniature robot upon repeated bending in deionized water (0% ethanol) and 100% ethanol (Figure 4d and Video S1). As a result, the shape morphing of the soft miniature robot was maintained at 1.77 ± 0.14 mm even after 14 cycles (Figure 4e). Additionally, reversible shape morphing of the soft miniature robot in deionized water (0% ethanol) and 100% ethanol were achieved within about 8.1 s (Figure 4e). These results demonstrate that the proposed soft miniature robot can control the bending curvature according to the amount of water absorption and has high durability to withstand repeated bending. Furthermore, through the obtained bending curvature results, we confirmed that the soft miniature robot has a structure and bending performance suitable for transporting microbeads.

3.3. Magnetic-Field-Actuated Shape-Morphing Test of Soft Miniature Robot

Along with the hydrogel swelling, the soft miniature robot was fabricated to be shape-morphable by external magnetic fields. This shape morphing occurs because the soft robot contains sufficient MNPs whose structure can be deformed by external magnetic fields. Therefore, we aim to manipulate the bead as desired using the shape morphing of the soft robot by the external magnetic fields (Figure 5a).

To evaluate the soft miniature robot's magnetic-field-actuated shape morphing, we applied various intensities of external magnetic fields to the soft miniature robot. The magnetic field intensity was controlled by changing the distance between the neodymium permanent magnet and the soft robot (Figure 5b). As a result, we confirmed that the magnetic field intensity varied from about 25 mT to 365 mT, with respect to the distance (from a maximum of 11 mm to a minimum of 0 mm) (Figure 5c). Under various magnetic field intensities, the soft miniature robot showed no shape change up to a distance of 5 mm from the magnet but a rapid shape deformation from 3 mm to 0 mm (Figure 5d). Specifically, the shape change in the soft miniature robot ranged from 0.14 mm to 1.68 mm from the distance of 3 mm to 0 mm from the magnet (Figure 5e). In particular, when the distance between the magnet and the soft robot was 0 mm, the soft miniature robot was fully unfolded. Here, the soft miniature robot unfolds fully through hydrogel-swelling and magnetic-field actuation, reaching a point where the magnetic force and restoring force are balanced. These results imply that sufficient shape morphing for a soft miniature robot to grasp a desired object can be achieved via wireless actuation by external magnetic fields. Next, we evaluated the repeatability of shape morphing of the soft miniature robot under external magnetic fields. We confirmed that the soft miniature robot stably maintained shape morphing without structural damage when the distance between the magnet and the soft robot was varied three times (Figure 5f,g). These results demonstrate that the proposed soft miniature robot has sufficient magnetic-field-driven force to overcome bending deformation by hydrogel swelling and is durable enough to withstand repeated magnetically actuated shape morphing.

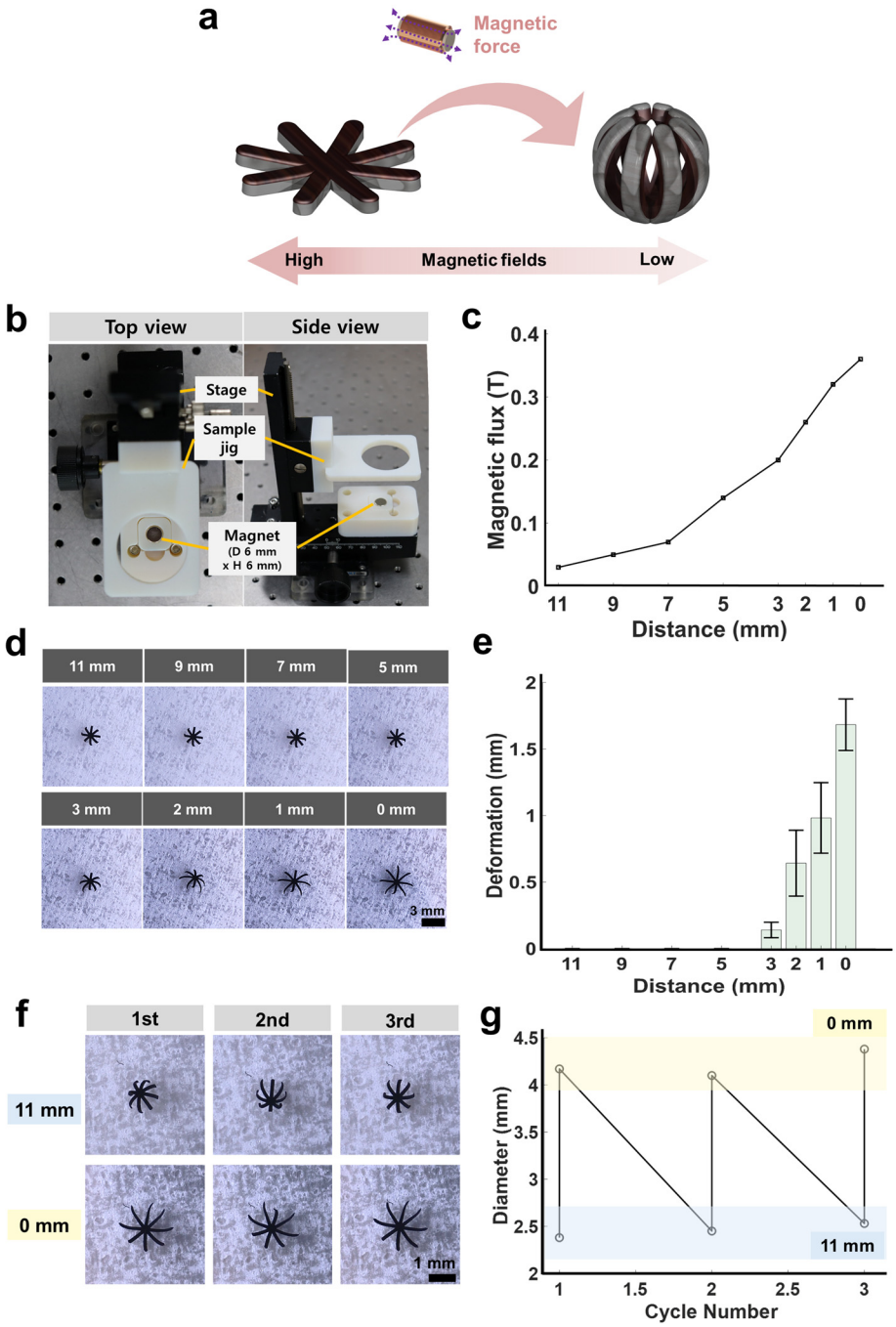

Figure 5. Magnetic-field-actuated shape-morphing performance of the soft miniature robot. (**a**) Schematic illustration of magnetic-fields-actuated shape morphing of the soft miniature robot. (**b**) Experimental setup for the shape-morphing test of the soft miniature robot. (**c**) Measured magnetic field intensity as a function of distance from a permanent magnet. (**d**) Optical images and (**e**) graph showing the shape morphing of the soft miniature robot according to the distance from the magnet. (**f**) Optical images and (**g**) graph of cyclic stability of the curvature of the soft miniature robot according to the distance from the magnet.

3.4. Magnetic-Field-Driven Mobility Test of Soft Miniature Robot

Before evaluating the bead gripping and targeting of the soft miniature robot, we tested the mobility of the soft miniature robot under external magnetic fields generated by an ENS. The ENS can generate uniform magnetic fields of up to 30 mT in the workspace in a desired direction in three-dimensional (3D) space. Therefore, by using the rotating

magnetic fields generated from the ENS, the soft miniature robot can realize rolling motion through the rolling friction between the robot and the surface.

Using an experimental setup including the ENS (Figure 6a,b), we investigated the mobility of a soft miniature robot in phosphate-buffered saline (PBS) under various magnetic field intensities (5, 20, and 30 mT) and rotational frequencies (0.5, 1, 3, 5, 7, 10, 15, 20, and 30 Hz) (Figure 6c–h). Regarding rotational frequency, the rolling speed of the soft miniature robot increased linearly in the frequency range from 0.5 Hz to 10 Hz, and the soft miniature robot reached the maximum speed of about 22 mm/s at about 10 Hz. Above 20 Hz, the frequency of the rotating magnetic field became higher than the step-out frequency of the soft miniature robot, and as a result, the speed of the soft miniature robot gradually decreased [26,27]. This phenomenon occurs almost similarly in the mobility of the soft miniature robot regardless of the strength of the magnetic field. Meanwhile, since the soft miniature robot has a high magnetization strength in a strong external magnetic field, it has a high magnetic torque and force even at the same frequency. As a result, the step-out frequency of the soft miniature robot increases from 10 Hz at an external magnetic field strength of 5 mT to 20 Hz at 30 mT.

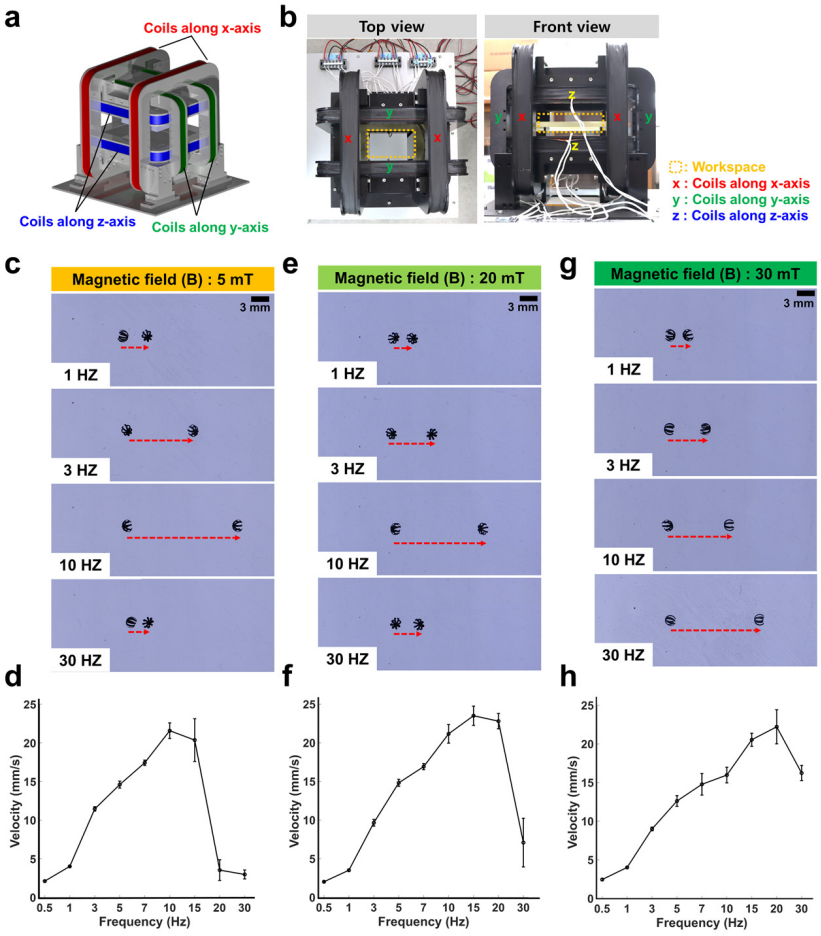

Figure 6. Magnetic-field-driven mobility of the soft miniature robot. (**a**) Design and (**b**) experimental setup of the ENS for magnetic-fields-driven mobility test of soft miniature robot. (**c**–**h**) Images and graphs showing the velocity of the soft minute robot in one second according to the rotating magnetic field strength and frequency. (**c**,**d**) 5 mT, (**e**,**f**) 20 mT, and (**g**,**h**) 30 mT.

3.5. Bead Gripping and Targeted Delivery Test of Soft Miniature Robot

Using the rolling motion of the soft miniature robot, we evaluated its mobility along a desired path by guiding it with an external magnetic field. As shown in Figure 7a and Video S2, the soft miniature robot was manipulated along a desired pattern under a rotating

magnetic field of 20 mT and 1 Hz. The result demonstrates that the proposed soft miniature robot can move with the desired speed, direction, and position by controlling the external magnetic field.

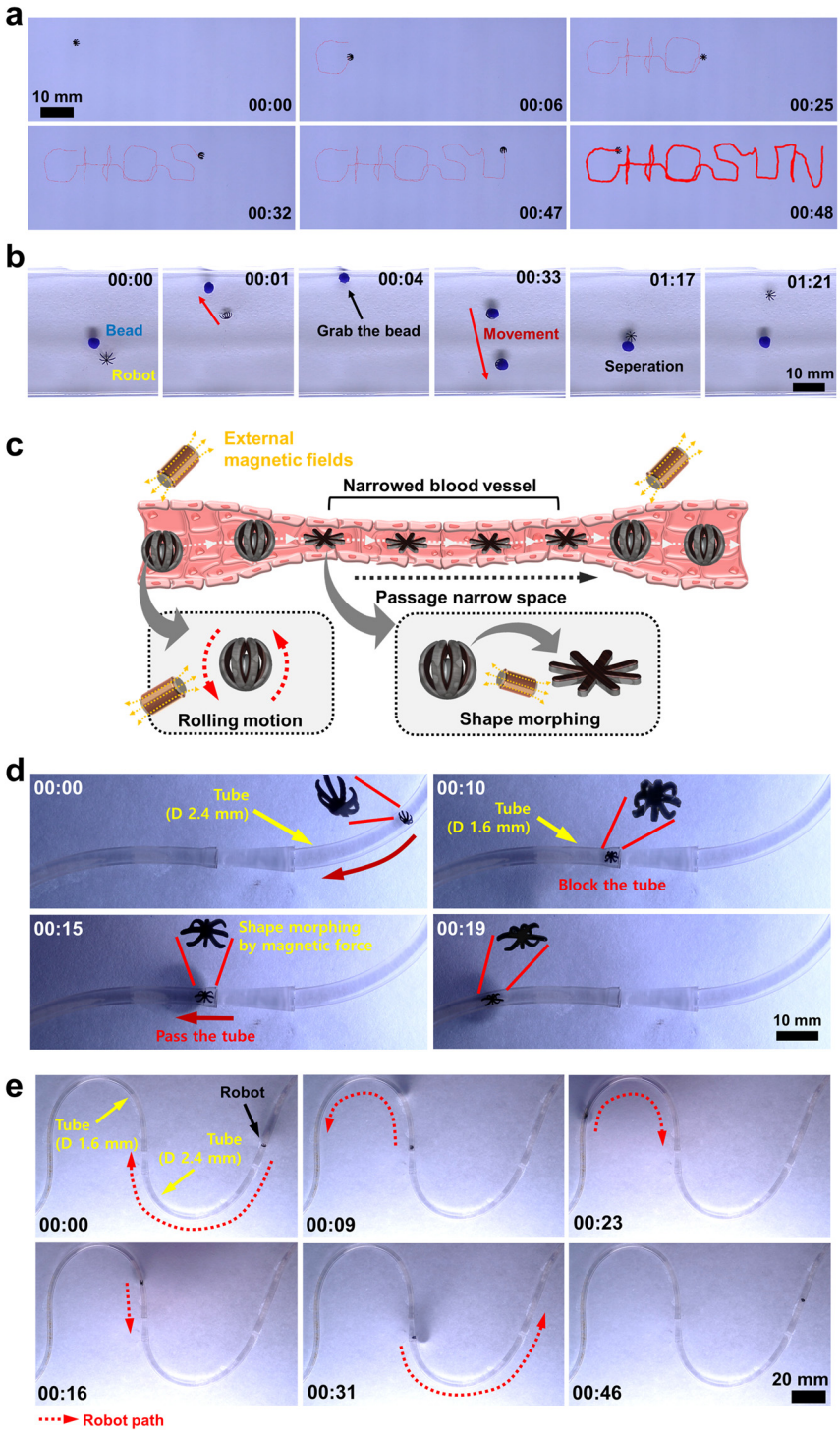

Figure 7. Bead gripping and targeted delivery of soft miniature robot. (**a**) Magnetic rolling locomotion of the soft miniature robot along a pre-selected pattern ('CHOSUN'). (**b**) Bead manipulation (gripping, delivery, and release) using the soft miniature robot under teleoperated magnetic field control. (**c**) Schematic illustration and (**d**,**e**) snapshots showing magnetic-fields-actuated shape morphing and locomotion of a soft miniature robot in a channel connected by tubes of different sizes. In all figures, the time is indicated on each figure in the minutes/seconds format.

As a proof of concept, we demonstrated the trapping, delivery, and release of an alginate bead using a soft miniature robot under teleoperation (Figure 7b and Video S3). First, the soft miniature robot, folded by hydrogel swelling, was guided to an alginate bead while unfolding under a strong magnetic force from a permanent magnet. Then, the unfolded soft miniature robot folded under the weakened magnetic force and gripped the alginate bead. The soft miniature robot moved freely without releasing alginate beads under external magnetic fields. After the magnetic guidance of the soft miniature robot, the alginate bead was released when the soft robot unfolded again under the applied strong magnetic force.

Next, to verify that the proposed soft miniature robot moves through complex and narrow blood vessels, we performed magnetic guidance of the soft miniature robot in a channel where tubes of various sizes are connected (Figure 7c). As shown in Figure 7d and Video S4, the soft miniature robot freely moved through a tube with a larger diameter (2.4 mm) than its size (about 2.22 mm) using rolling motion via rotating magnetic fields with weak intensity. Then, the soft miniature robot reaches a tube with a smaller diameter (1.6 mm) that cannot pass through by rolling motion using rotating magnetic fields. To pass through this narrow space, the soft miniature robot deformed into a shape smaller than the tube using stronger magnetic field intensity than rotating magnetic fields. As a result, the magnetic shape deformation of the soft miniature robot enabled it to pass through the small tube. Furthermore, the soft miniature robot moved through the curved tube and stably returned from the narrow tube to the wide tube (Figure 7e and Video S5). These results indicate that the proposed soft miniature robot can not only grip an object and release it at a desired location but also be precisely magnetically guided through a complex and narrow space by an external magnetic field.

3.6. Discussion

Regarding the shape morphing of the soft robot, the proposed soft miniature robot with eight arms has a maximum bending curvature, angle, and response time of ~2 mm, 140°, and ~8.1 s, respectively, due to the hydrogel-swelling actuation. These features enable the robot to effectively trap microbeads without unintended release. In addition, compared with the existing biomaterial-based soft miniature robots [18–20], the proposed soft miniature robot has a high bending performance (Figure S1). To overcome the high bending curvature caused by the hydrogel-swelling actuation, the soft miniature robot requires an external magnetic field of at least 200 mT. Furthermore, an external magnetic field of 365 mT is needed to fully unfold the soft miniature robot. While the rolling motion of the soft miniature robot was realized with an external magnetic field of 5 mT, the shape morphing requires an external magnetic field of at least 40 times that strength. These results indicate that a significantly strong magnetic force is necessary to overcome the bending stiffness of the soft miniature robot. To achieve shape morphing of soft miniature robots inside the body, the ENS that generates a strong external magnetic field is necessary. However, there are limitations in terms of space and cost to operate an ENS with a large volume and high power consumption only for targeted drug delivery based on soft miniature robots. To overcome these limitations, we will design a structure of a soft miniature robot that can implement shape morphing under a weak magnetic field. As another alternative, we will utilize the material of a soft miniature robot that can selectively release drug beads in vivo by external energy stimulation other than an external magnetic field.

Next, in terms of magnetic-field-driven mobility, the proposed soft miniature robot has a speed (~3.1 body length/stroke) that is three times faster than that of the existing soft miniature robot with a similar shape (~0.95 body length/stroke) [20]. In addition, the maximum speed of the soft miniature robot is about 22 mm/s, which is similar to the blood flow velocity of 2 mL/min (~22 mm/s) in the branch diameter (~4.1 mm) [28]. Therefore, we expect that the mobility of the soft miniature robot will be sufficient to target the desired blood vessel in the branch except for the movement against the blood flow. In future work,

we will verify the magnetic guidance of the soft miniature robot to the target blood vessel in a phantom mimicking human blood vessels. Furthermore, we will test the in vivo targeting of the soft miniature robot in narrow, fluid-filled spaces, such as animal blood vessels, bile ducts, and articular cavities.

4. Conclusions

This study reports a wirelessly hybrid-actuated soft miniature robot for biomedical applications. The soft miniature robot composed of chitosan and MNPs was fabricated into a desired shape by laser micromachining. The proposed soft miniature robot exhibited shape morphing and magnetic locomotion through hydrogel-swelling and magnetic-field actuation, respectively. The shape morphing of the soft miniature robot was evaluated by measuring the bending curvature according to magnetic force and water absorption. Furthermore, the mobility of the soft miniature robot was verified through a rolling locomotion test according to the strength and frequency of an external rotating magnetic field. Finally, the feasibility of the proposed soft miniature robot in biomedical applications was verified through tests such as gripping and releasing a single alginate bead and targeted delivery using magnetic guidance in a channel. This study shows that the new soft miniature robot performs better at bending than existing biomaterial-based soft miniature robots. Additionally, the robot's magnetic actuation allows it to change shape without causing damage to its body. As a result, this study demonstrates that this soft miniature robot can be accurately directed to hard-to-reach areas within the body, which has yet to be reported with existing biomaterial-based soft miniature robots. Although we proposed a soft robot for biomedical applications in this study, much effort is required to verify biocompatibility, biodegradability, and targeted drug delivery beyond in vitro and phantom tests to advance to in vivo tests. Regarding biocompatibility and biodegradability, soft miniature robots in the body are located in the disease, but degraded by-products circulate throughout the body through the blood. The soft miniature robot and degraded by-products may cause inflammation or form thrombosis in the body. Therefore, the biocompatibility and biodegradability of soft miniature robots should be verified through cell viability, inflammatory responses in body organs, and thrombogenicity. Next, in in vivo targeted drug delivery, the magnetic mobility of the soft miniature robot may reduce the precision of movement to the target site because the body fluid has high viscosity or flow velocity. Therefore, the soft miniature robot needs real-time imaging-based precision navigation considering various vascular branches and blood flow in the body. In addition, the magnetic-field-actuated shape morphing of the proposed soft miniature robot requires a strong magnetic field. Thus, the in vivo shape morphing of the soft robot should be verified in various organs in the body, such as the blood vessels, bile ducts, and articular cavities of animals. The defects and limitations of the soft robot identified through the in vivo shape-morphing test should be improved through material and structural design. Through the research efforts, we expect that the proposed soft miniature robot can ultimately be used with therapeutics to enable precision-guided targeted delivery.

Supplementary Materials: The following supporting information can be downloaded at: https://www.mdpi.com/article/10.3390/act13090341/s1, Video S1: Hydrogel swelling actuated bending of the soft miniature robot in deionized water (0% ethanol) and 100% ethanol; Video S2: Magnetic rolling locomotion of the soft miniature robot along a pre-selected pattern ('CHOSUN'); Video S3: Bead manipulation (gripping, delivery, and release) using the soft miniature robot; Video S4: Passage of narrow space of a soft miniature robot in a channel; Video S5: Magnetic field actuated shape morphing and locomotion of a soft miniature robot in a channel; Figure S1: State-of-art of soft miniature robots for biomedical applications; Figure S2: Pros and cons of external stimuli methods of soft miniature robot; Figure S3: Schematic diagram to illustrate the fabrication step of the soft miniature robot.

Author Contributions: Conceptualization, H.K., K.L. and G.G.; formal analysis, H.K.; investigation, H.K. and K.L.; writing—original draft preparation, H.K., K.L. and G.G.; writing—review and editing,

G.G.; visualization, H.K. and K.L.; supervision, G.G.; project administration, G.G.; funding acquisition, G.G. All authors have read and agreed to the published version of the manuscript.

Funding: This study was supported by research fund from Chosun University, 2023.

Data Availability Statement: The original contributions presented in the study are included in the article/Supplementary Material, further inquiries can be directed to the corresponding author/s.

Acknowledgments: We thank the Medical Microrobot Center at Chonnam National University for providing facilities.

Conflicts of Interest: The authors declare no conflicts of interest.

References

1. Rich, S.I.; Wood, R.J.; Majidi, C. Untethered soft robotics. *Nat. Electron.* **2018**, *1*, 102–112. [CrossRef]
2. Rus, D.; Tolley, M.T. Design, fabrication and control of soft robots. *Nature* **2015**, *521*, 467–475. [CrossRef] [PubMed]
3. Laschi, C.; Mazzolai, B.; Cianchetti, M. Soft robotics: Technologies and systems pushing the boundaries of robot abilities. *Sci. Robot.* **2016**, *1*, eaah3690. [CrossRef] [PubMed]
4. Mazzolai, B.; Mondini, A.; Del Dottore, E.; Margheri, L.; Carpi, F.; Suzumori, K.; Cianchetti, M.; Speck, T.; Smoukov, S.K.; Burgert, I.; et al. Roadmap on soft robotics: Multifunctionality, adaptability and growth without borders. *Multifunct. Mater.* **2022**, *5*, 032001. [CrossRef]
5. Bang, J.; Choi, S.H.; Pyun, K.R.; Jung, Y.; Hong, S.; Kim, D.; Lee, Y.; Won, D.; Jeong, S.; Shin, W.; et al. Bioinspired electronics for intelligent soft robots. *Nat. Rev. Electr. Eng.* **2024**. [CrossRef]
6. Cianchetti, M.; Laschi, C.; Menciassi, A.; Dario, P. Biomedical applications of soft robotics. *Nat. Rev. Mater.* **2018**, *3*, 143–153. [CrossRef]
7. Wang, T.; Wu, Y.; Yildiz, E.; Kanyas, S.; Sitti, M. Clinical translation of wireless soft robotic medical devices. *Nat. Rev. Bioeng.* **2024**, *2*, 470–485. [CrossRef]
8. Hines, L.; Petersen, K.; Lum, G.Z.; Sitti, M. Soft Actuators for Small-Scale Robotics. *Adv. Mater.* **2017**, *29*, 1603483. [CrossRef]
9. Manduca, G.; Santaera, G.; Miraglia, M.; Jansen Van Vuuren, G.; Dario, P.; Stefanini, C.; Romano, D. A Bioinspired Control Strategy Ensures Maneuverability and Adaptability for Dynamic Environments in an Underactuated Robotic Fish. *J. Intell. Robot. Syst.* **2024**, *110*, 69. [CrossRef]
10. Lalegani Dezaki, M.; Bodaghi, M. A Review of Recent Manufacturing Technologies for Sustainable Soft Actuators. *Int. J. Precis. Eng. Manuf.-Green Technol.* **2023**, *10*, 1661–1710. [CrossRef]
11. Ma, S.; Xue, P.; Tang, Y.; Bi, R.; Xu, X.; Wang, L.; Li, Q. Responsive soft actuators with MXene nanomaterials. *Responsive Mater.* **2024**, *2*, e20230026. [CrossRef]
12. Fusco, S.; Huang, H.-W.; Peyer, K.E.; Peters, C.; Häberli, M.; Ulbers, A.; Spyrogianni, A.; Pellicer, E.; Sort, J.; Pratsinis, S.E.; et al. Shape-Switching Microrobots for Medical Applications: The Influence of Shape in Drug Delivery and Locomotion. *ACS Appl. Mater. Interfaces* **2015**, *7*, 6803–6811. [CrossRef]
13. Mariani, S.; Cecchini, L.; Mondini, A.; Del Dottore, E.; Ronzan, M.; Filippeschi, C.; Pugno, N.M.; Sinibaldi, E.; Mazzolai, B. A Bioinspired Plasmonic Nanocomposite Actuator Sunlight-Driven by a Photothermal-Hygroscopic Effect for Sustainable Soft Robotics. *Adv. Mater. Technol.* **2023**, *8*, 2202166. [CrossRef]
14. Zhang, J.; Wang, Y.; Sun, Y.; Sun, S.; Xu, Z.; Li, J.; Li, J.; Gong, X. Multi-Stimuli Responsive Soft Actuator with Locally Controllable and Programmable Complex Shape Deformations. *ACS Appl. Polym. Mater.* **2023**, *5*, 6199–6211. [CrossRef]
15. Hu, W.; Lum, G.Z.; Mastrangeli, M.; Sitti, M. Small-scale soft-bodied robot with multimodal locomotion. *Nature* **2018**, *554*, 81–85. [CrossRef] [PubMed]
16. Dong, Y.; Wang, J.; Guo, X.; Yang, S.; Ozen, M.O.; Chen, P.; Liu, X.; Du, W.; Xiao, F.; Demirci, U.; et al. Multi-stimuli-responsive programmable biomimetic actuator. *Nat. Commun.* **2019**, *10*, 4087. [CrossRef] [PubMed]
17. Zheng, Z.; Han, J.; Demir, S.O.; Wang, H.; Jiang, W.; Liu, H.; Sitti, M. Electrodeposited Superhydrophilic-Superhydrophobic Composites for Untethered Multi-Stimuli-Responsive Soft Millirobots. *Adv. Sci.* **2023**, *10*, 2302409. [CrossRef]
18. Malachowski, K.; Jamal, M.; Jin, Q.; Polat, B.; Morris, C.J.; Gracias, D.H. Self-Folding Single Cell Grippers. *Nano Lett.* **2014**, *14*, 4164–4170. [CrossRef]
19. Kobayashi, K.; Yoon, C.; Oh, S.H.; Pagaduan, J.V.; Gracias, D.H. Biodegradable Thermomagnetically Responsive Soft Untethered Grippers. *ACS Appl. Mater. Interfaces* **2019**, *11*, 151–159. [CrossRef]
20. Goudu, S.R.; Yasa, I.C.; Hu, X.; Ceylan, H.; Hu, W.; Sitti, M. Biodegradable Untethered Magnetic Hydrogel Milli-Grippers. *Adv. Funct. Mater.* **2020**, *30*, 2004975. [CrossRef]
21. Nan, M.; Go, G.; Song, H.-W.; Darmawan, B.A.; Zheng, S.; Kim, S.; Nguyen, K.T.; Lee, K.; Kim, H.; Park, J.-O.; et al. Multistimulus-Responsive Miniature Soft Actuator with Programmable Shape-Morphing Design for Biomimetic and Biomedical Applications. *Adv. Funct. Mater.* **2024**, *34*, 2401776. [CrossRef]
22. Krishnaveni, B.; Ragunathan, R. Extraction and characterization of Chitin and Chitosan from Aspergillus terreus sps, synthesis of their bionanocomposites and study of their productive applications. *J. Chem. Pharm. Res.* **2015**, *7*, 115–132.

23. Go, G.; Yoo, A.; Song, H.-W.; Min, H.-K.; Zheng, S.; Nguyen, K.T.; Kim, S.; Kang, B.; Hong, A.; Kim, C.-S.; et al. Multifunctional Biodegradable Microrobot with Programmable Morphology for Biomedical Applications. *ACS Nano* **2021**, *15*, 1059–1076. [CrossRef] [PubMed]
24. Fernandes Queiroz, M.; Melo, K.R.; Sabry, D.A.; Sassaki, G.L.; Rocha, H.A. Does the Use of Chitosan Contribute to Oxalate Kidney Stone Formation? *Mar. Drugs* **2015**, *13*, 141–158. [CrossRef]
25. Go, G.; Yoo, A.; Nguyen, K.T.; Nan, M.; Darmawan, B.A.; Zheng, S.; Kang, B.; Kim, C.-S.; Bang, D.; Lee, S.; et al. Multifunctional microrobot with real-time visualization and magnetic resonance imaging for chemoembolization therapy of liver cancer. *Sci. Adv.* **2022**, *8*, eabq8545. [CrossRef]
26. Diller, E.; Giltinan, J.; Sitti, M. Independent control of multiple magnetic microrobots in three dimensions. *Int. J. Robot. Res.* **2013**, *32*, 614–631. [CrossRef]
27. Mahoney, A.W.; Nelson, N.D.; Peyer, K.E.; Nelson, B.J.; Abbott, J.J. Behavior of rotating magnetic microrobots above the step-out frequency with application to control of multi-microrobot systems. *Appl. Phys. Lett.* **2014**, *104*, 144101. [CrossRef]
28. Debbaut, C.; Segers, P.; Cornillie, P.; Casteleyn, C.; Dierick, M.; Laleman, W.; Monbaliu, D. Analyzing the human liver vascular architecture by combining vascular corrosion casting and micro-CT scanning: A feasibility study. *J. Anat.* **2014**, *224*, 509–517. [CrossRef]

Disclaimer/Publisher's Note: The statements, opinions and data contained in all publications are solely those of the individual author(s) and contributor(s) and not of MDPI and/or the editor(s). MDPI and/or the editor(s) disclaim responsibility for any injury to people or property resulting from any ideas, methods, instructions or products referred to in the content.